Methane Hydrate Dissociation by Depressurization in a Mount Elbert Sandstone Sample: Experimental Observations and Numerical Simulations

Timothy J. Kneafsey and George J. Moridis SPE/Lawrence Berkeley National Laboratory

Abstract

A preserved sample of hydrate-bearing sandstone from the Mount Elbert Test Well was dissociated by depressurization while monitoring the internal temperature of the sample in two locations and the density changes at high spatial resolution using x-ray CT scanning. The sample contained two distinct regions having different porosity and grain size distributions. The hydrate dissociation occurred initially throughout the sample as a result of depressing the pressure below the stability pressure. This initial stage reduced the temperature to the equilibrium point, which was maintained above the ice point. After that, dissociation occurred from the outside in as a result of heat transfer from the controlled temperature bath surrounding the pressure vessel. Numerical modeling of the test using TOUGH+HYDRATE yielded a gas production curve that closely matches the experimentally measured curve.

Introduction

Recent studies have concluded that methane hydrate (hereafter hydrate), a naturally occurring clathrate compound consisting of molecular water cages surrounding gas molecules (primarily methane), contains large quantities of methane in shallow sediments throughout the world's coastal margins and polar regions [*Boswell et al.*, 2010; *Milkov*, 2004; *Sloan et al.*, 1998]. Each cubic meter of hydrate can hold approximately 160 m^3 of natural gas at standard temperature and pressure [*National Resource Council*, 2004]. Even though natural gas from hydrate shows great promise as an energy resource, scientific and engineering questions remain regarding producing gas from hydrates. Three methods are typically considered to produce gas from hydrate: depressurization, where the system pressure is lowered below the hydrate stability pressure; thermal stimulation, where the hydrate-bearing sediments are heated to temperatures in excess of the hydrate stability temperature, and the use of inhibitors such as sodium chloride or alcohols that modify the hydrate stability conditions to destabilize the hydrate [*Sloan and Koh*, 2008]. Of these techniques, heating the hydrate-bearing sediments and injecting expensive alcohols or corrosive brines may have limited applications, but will often be impractical, particularly considering the size of reservoirs and the lack of control that can be exerted to directly apply the heat or inhibitor to the location needed. Depressurization is expected to be effective in many situations, however the hydrate-bearing sediments must be well enough confined by low permeability strata for the depressurization to be effective. Many suboceanic deposits are thought to contain hydrate in low abundance over large regions, in low permeability clays or fine grain sediments, or in strata that are well connected to moderate permeability zones that make gas production impractical [*Moridis and Sloan*, 2007]. Known deposits of methane hydrate are present in regions beneath the north slope of the Brooks Range where conditions are suitable for methane hydrate occurrence. These hydrate-bearing strata are confined by low-permeability layers [*Boswell et al.*, 2010], making depressurization the apparent method for production.

After careful evaluation of geophysical and well log data, the BPXADOE-USGS Mount Elbert Gas Hydrate Stratigraphic Test Well (Mount Elbert Well) was drilled in February 2007 [*Hunter et al.*]. This drilling and coring operation allowed comparison of predicted and actual subsurface lithology including the presence and saturation of hydrate, provided a detailed description of the lithology, pore water chemistry, and gas composition, and retrieved hydrate-bearing cores for analysis and testing. These data, along with predictions of the expected conditions, provide an opportunity to compare predictions to as-found conditions and refine prediction tools, as well as provide input information for simulating possible natural gas extraction from this region.

In that effort, we have performed an experiment in which we have performed a controlled dissociation by depressurization of a preserved hydrate-bearing sample from the Mount Elbert Well, and have also simulated this process using TOUGH+HYDRATE [Moridis et al., 2008]. The TOUGH+HYDRATE code has been developed to evaluate hydrate-related questions, including methane release upon climate change

and the production of gas from gas hydrates. Comparison of simulator predictions to analytical solutions, field data, and laboratory data is needed to build confidence in the model. In this paper, we describe the production of methane from the hydrate present in a core from the Mount Elbert Well. We monitored temperatures and pressures in our controlled depressurization test, and monitored location specific behavior using X-ray computed tomography (CT). We simulated our production test using TOUGH+HYDRATE and compare the results of the experiment and simulation.

Method

Sample Description

The two-region core sample (HYPV4, from 663.89 to 664.14 m depth; 2178.12 to 2178.92 ft depth) was collected during the coring performed on the Mount Elbert Stratigraphic Test Well during February 2007. A description of the coring and collection is contained in Kneafsey et al. (2009a). Briefly, coring was performed using a chilled custom oil-based mud to aid in sample preservation, however pressure-coring techniques were not used. The sample studied in our test was one of several that were retrieved, cut to 10-inch length, scraped clean, wrapped in aluminum foil, and placed in pressure vessels (Parr Instruments, Moline, IL) which were pressurized to 5.52 MPa (800 psi) with 99.99% pure methane gas. The vessels were kept at temperatures ranging from -40^{o}C to -4^{o}C. Prior to shipping from the well site, the vessels were inspected and it was noted that pressures had decreased (presumably from cooling, small gas leaks in the vessel seals or valves, or by hydrate formation, as the samples were maintained at pressures well within the hydrate stability zone), and the vessels were repressurized to 6.20 MPa (900 psi) then shipped overland to Anchorage, Alaska. Temperatures during transportation in late February ranged from -40 to -10 degrees C. After arrival in Anchorage, the pressurized core samples were stored in a refrigerated container maintained at -7^{o}C. Prior to further shipping, the pressure vessels, which were again noted to be below the initial pressure, were rapidly depressurized (in about 1 minute), the samples removed, labeled, placed into cloth bags and immersed in LN (taking 3-6 minutes).

Experiment Description

To perform the depressurization dissociation experiment, a cylindrical portion of the core had to be properly machined and inserted into a elastomer sleeve between two endpieces, which then had to be inserted into an x-ray transparent pressure vessel, have confining and pore pressures applied at controlled temperatures with minimum core disturbance and minimum hydrate dissociation. The core was received in a dry-ship dewar at the liquid nitrogen (LN) boiling point (-196^{o}C). At this temperature, the hydrate is stable at atmospheric pressure.

The core sample was machined to fit the custom sleeve by intermittently removing it from the LN, rapidly performing an operation (e.g. briefly sanding a side or drilling a hole) and returning it to the LN to cool it prior to the next machining step. When machining, the sample was set on an insulator, rather than the steel tool tables to reduce sample warming. When machining was completed and the sample had been re-chilled to -196^{o}C, it was inserted into the custom nitrile sleeve, which had been mounted to a PVC endpiece having a thermocouple extending through the center. The opposing PVC endpiece with a thermocouple extending through the center was rapidly inserted and attached, and the assembly was sealed within the pressure vessel filled with a water/ propylene glycol mixture chilled to about -30^{o}C. Immediately, confining pressure was applied and the pore pressure was controlled. The temperature of the pressure vessel was controlled by flowing chilled propylene glycol/water through the PVC jacket surrounding the aluminum vessel. A schematic of the system is shown in Figure 1 and three cross sections of the sample are shown in Figure 2 to show the structure of the PVC endpiece, and the locations of the thermocouples.

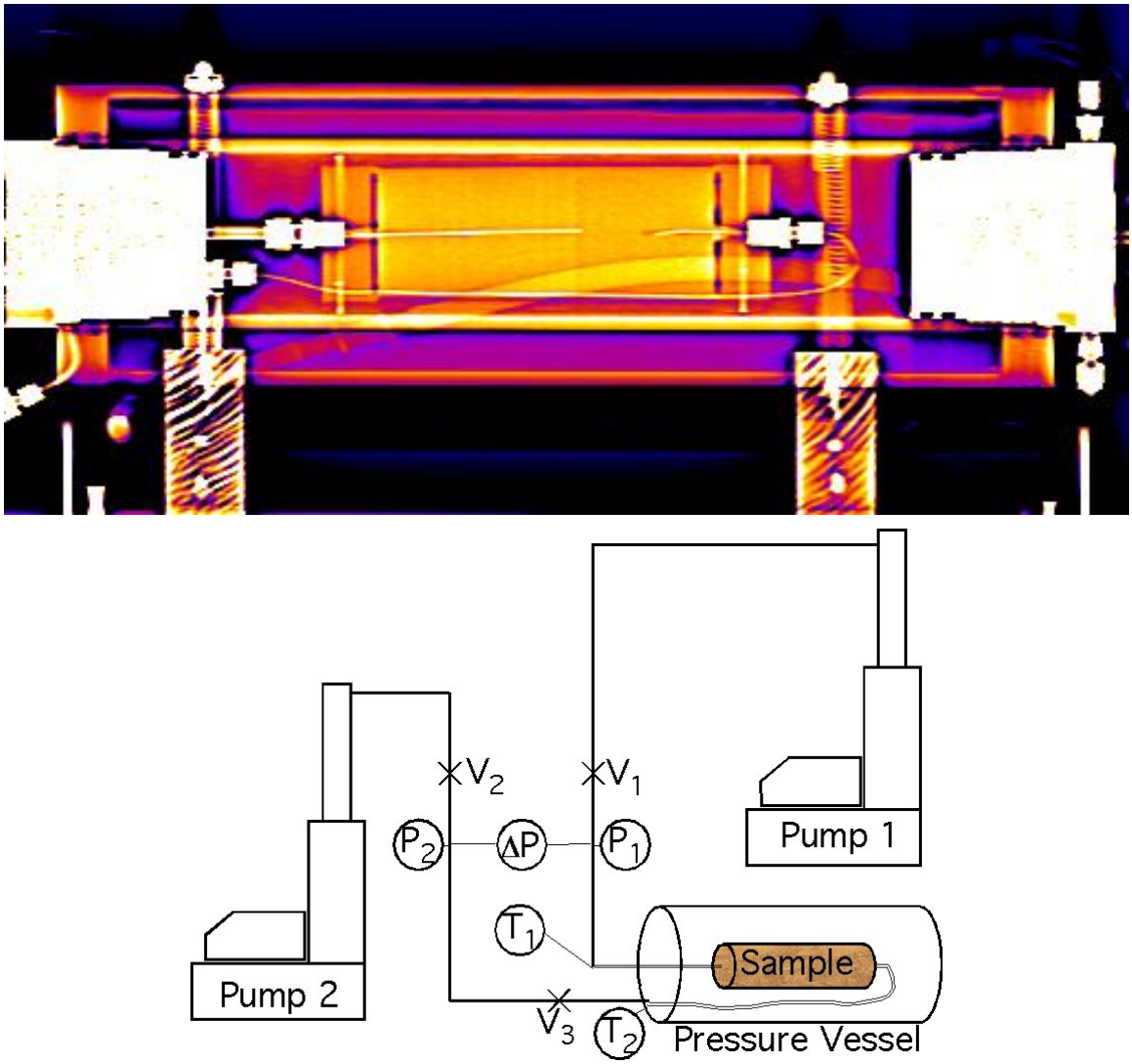

Figure 1. top. X-ray image of experimental setup. bottom. Schematic of setup.

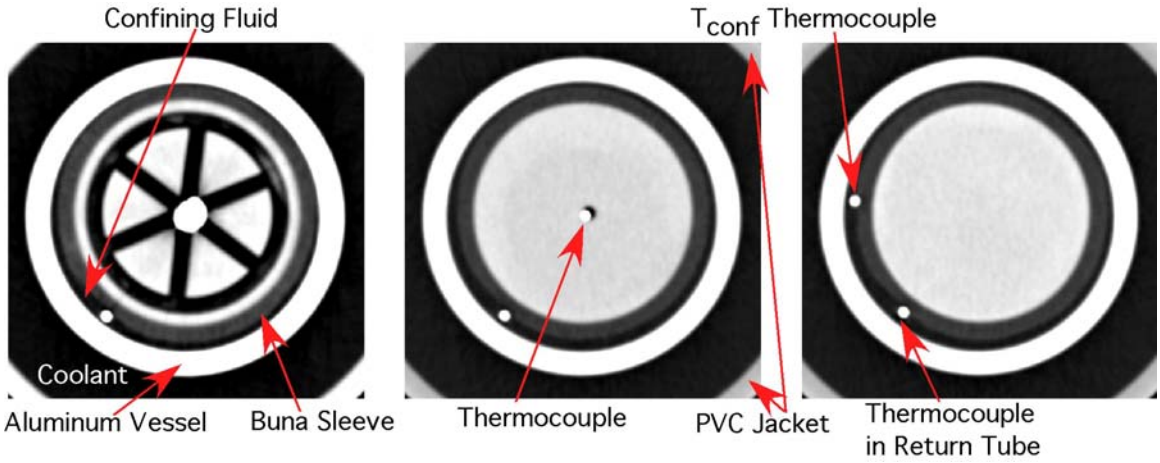

Figure 2. a. Machined PVC endpiece for fluid distribution, b. Typical cross section with thermocouple in center, c. Typical cross section showing location of the confining fluid thermocouple

As the core warmed from -196 ^{o}C, the confining pressure was increased so that it always exceeded the pore pressure of the sample. The sample was slowly warmed to the experiment temperature, and then the experiment system was equilibrated at about 570 psig and 4.27C. While the temperature was still below 0^{o}C, the assembly was scanned using a modified Siemens Somatom HiQ X-ray computed tomography (CT) scanner. CT scanning revealed that the sample spanned across two strata having different porosities (Figure 3). Subsequent analysis of subsamples from each end revealed that each side had a different grain size distribution as well, but similar mineralogy (Table 1).

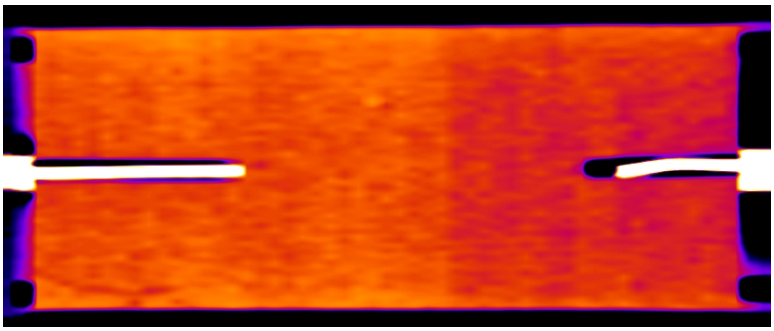

Figure 3. X-ray CT cross-section through the frozen core. In this image, brighter colors represent higher density, and darker colors represent lower density. Two regions are clearly visible.

Table 1. Properties of the two regions of the core

	Region A (left in Figures 1, 3)	Region B (right in Figures 1, 3)
Average Porosity (from CT)	.337	.353
Approximate Hydrate Saturation (as received)	.23	.42

The inlet and outlet of the sample were connected to high-pressure syringe pumps (Teledyne Isco, Lincoln NE) containing methane. Prior to the depressurization test, we attempted to flow gas through the sample in order to assess its effective permeability. Under reasonable conditions, no gas flowed through the sample, thus the effective permeability was quite low. After resetting the pressure to 570 psi, and the core was shut in. The lines between the control valves and the pumps on both sides of the core and the high pressure syringe pumps were set to maintain 445 psig, and Pump2 was isolated from the system at valve V2. To depressurize the sample, valves V1 and V3 were opened.

The Numerical Models and Simulation Approach

The numerical simulation code

We used the serial and parallel versions of the TOUGH+HYDRATE simulator (Moridis et al., 2008; Zhang et al., 2008) to conduct the numerical studies in this paper. This code (hereafter referred to as T+H) can model all the known processes involved in the response of the CH_4+H_2O system to pressure and temperature changes in the pores and fractures of complex geologic media, including the flow of fluids and heat, the thermophysical properties of reservoir fluids, thermodynamic changes and phase behavior, and the non-isothermal chemical reaction of CH_4-hydrate formation and/or dissociation, which can be described by either an equilibrium or a kinetic model (Kim et al., 1998; Clarke and Bishnoi, 2001; Kowalsky and Moridis, 2007). T+H is a compositional simulator, and its formulation accounts for heat and up to four mass components (i.e., H_2O, CH_4, CH_4-hydrate, and water-soluble inhibitors such as salts or alcohols) that are partitioned among four possible phases: gas, aqueous liquid, ice, and hydrate. The T+H code can describe all the 15 possible thermodynamic states (phase combinations) of the CH_4+H_2O system and any combination of the three main methods of hydrate dissociation, i.e., depressurization, thermal stimulation, and the effect of inhibitors.

System geometry and domain discretization.

The system investigated in this study is the experimental core assembly described above. The dimensions

of the system and of its various components (hydrate-bearing code, Buna sleeve, PVC end-caps, confining and heat-exchanging fluid, and the aluminum vessel) were the same as the experiment system. Note that the simulation domain was somewhat trimmed from the full system in that it was limited to (a) the part of the assembly between the outer edges of the PVC end-plates along the length of the core, and to the outer diameter of the aluminum vessel. This limited domain was considered adequate for an accurate representation of the system behavior because (a) the temperature of the confining liquid at the two PVC end-caps was treated as an input (as obtained from direct measurements), and (b) the temperature of the bath surrounding the aluminum vessel was known (also from direct measurements). Thus, imposing these two temperatures as boundary temperatures prevented erroneous computations that could have been caused by an inaccurate heat balance during the dissociation process.

For maximum accuracy, very fine grids were used in the simulation of production. Because gravity cannot be ignored due to the release of water during dissociation, a three-dimensional Cartesian grid was used to represent the simulated domain. Fortunately, only half of the domain needed to be simulated because of symmetry about the vertical (z-) plane. The 7.97 inch (=202.5 mm) of the core and PVC end-caps along the length of the core (x-direction) were subdivided into 83 segments, of which 81 of $\Delta x = 2.5$ mm in length, and the two outermost ones (representing the variable-temperature boundaries of the confining fluid) with $\Delta x = 1$ mm. Along the z-axis, the 3.5 inch (=88.9 mm) diameter of the domain was discretized into 52 subdivisions, of which:

- The outermost one corresponded to the liquid bath boundary, with a $\Delta z = 1$ mm;
- The next two cells (corresponding to the outer layers of the outer diameter of the aluminum vessel) had a $\Delta z = 1.18$ mm;
- The remainder of the metal vessel thickness was represented by 4 cells/layers of $\Delta z = 1$ mm
- The inside of the vessel including the hydrate-bearing core from z = 1.5" to z = 0" (= 38.1 mm in total) was discretized into a subdivision with $\Delta z = 2.1$ mm and 18 with $\Delta z = 2.0$ mm;
- The discretization of the lower half of the cylindrical assembly (i.e., from z = 0" to z = -1.5") was a mirror image of that of the upper half.

The discretization along the y-axis was the same as that in the upper (or lower) half of the z-direction. Because the Cartesian discretization described above was used to describe a cylindrical domain, a small program was written to (a) eliminate all cells outside the outermost cylindrical boundaries of the system, (b) adjust the surface area at the intersection/contact of different materials and subdomains to ensure correct heat exchange, and (c) adjust the boundary gridblock volumes to correctly reflect the actual system volume. Thus, the total number of gridblocks were reduced from 83x52x26 = 112,216 in (x,y,z) to 88,134, resulting in a system of 264,402 equations during the analysis of the hydrate dissociation problem.

System properties, initial and boundary conditions.

The initial and boundary conditions (pressure and temperature) were as described above and presented in Table 2. Of the other properties, the intrinsic permeability $k = 10^{-12}$ m^2 (= 1 darcy) was as determined from the history matching of data from an earlier field test of depressurization-induced hydrate dissociation at the Mt. Elbert site from which the core originated (Anderson et al., 2008; Moridis et al. 2010). The initial porosities ϕ and hydrate saturations S_H of the two regions of the core (Figure 3) were as determined from the CT scan analysis. The relative permeability relationships and the corresponding parameters were based on data obtained from history matching of the results of field test that had been conducted at the site (Anderson et al., 2008), and are shown in Table 2. The capillary pressure relationships and parameters were determined from the particle size analysis of porous media samples from the deeper (but similar) C unit (White, 2008) and were consistent with the ϕ and k of the formation (Table 2). Note that the same relative permeability and capillary pressure expressions and parameters were assumed to apply to both regions of the core. Finally, the thermal properties of the various components and subdomains of the system (Table 2) were obtained from various publications.

Table 2. Hydrate Deposit Properties in Unit D, Mount Elbert Site

Parameter	Value
Gas composition	100% CH_4
Medium compressibility of HBL	$5x10^{-9}$ Pa^{-1}
Intrinsic permeability $k_x = k_y = k_z$	10^{-12} m^2 (= 1 D)
Grain density ρ_R	2750 kg/m^3
Dry thermal conductivity ($k_{\Theta RD}$)	0.5 W/m/K
Wet thermal conductivity ($k_{\Theta RW}$)	3.1 W/m/K
Medium specific heat (C_Θ)	1000 J/kg/K
Aluminum 6061-T6 density	2700 kg/m^3
Alum. 6061-T6 thermal conductivity (k_Θ)	155 W/m/K
Alum. 6061-T6 specific heat (C_Θ)	1000 J/kg/K
Buna rubber density	860 kg/m^3
Buna thermal conductivity (k_Θ)	0.3 W/m/K
Buna specific heat (C_Θ)	2800 J/kg/K
PVC density	1220 kg/m^3
PVC thermal conductivity (k_Θ)	0.15 W/m/K
PVC specific heat (C_Θ)	880 J/kg/K
Composite thermal conductivity model (Moridis et al., 2008)	$k_{\Theta C} = k_{\Theta RD} + (S_A^{1/2} + S_H^{1/2})\,(k_{\Theta RW} - k_{\Theta RD}) + \phi\, S_I\, k_{\Theta I}$
Capillary pressure model (vanGenuchten, 1980)	$P_{cap} = -P_0 \left[\left(S^* \right)^{-1/\lambda} - 1 \right]^{\lambda}$ $S^* = \frac{(S_A - S_{irA})}{(S_{mxA} - S_{irA})}$
S_{irA}	1
λ (White, 2008)	0.77437
P_0 (White, 2008)	$5x10^3$ Pa
Relative permeability model (Moridis et al., 2008)	$k_{rA} = (S_A^*)^n$ $k_{rG} = (S_G^*)^m$ $S_A^* = (S_A - S_{irA})/(1 - S_{irA})$ $S_G^* = (S_G - S_{irG})/(1 - S_{irA})$ EPM model
n; m (from Anderson et al., 2008)	4.2; 2.5
S_{irG}	0.02
S_{irA}	0.20

Results

Experiment Results

The temperatures at three locations (two at the center of the core near the ends, and one in the confining fluid) and the differential pressure across the core are presented in Figure 4 for the depressurization test.

Upon opening valve V1 to begin the depressurization, the pressure on that side (for reference – left side) of the core dropped rapidly to the dissociation pressure (445 psig). The pressure on the opposite side (for reference - right side) increased towards the original system pressure as gas from the sample filled the tubing that had been depressurized to 445 psi(g), and then soon after began dropping towards the dissociation pressure. This resulted in a high pressure differential across the core (up to 95 psi) initially, which dropped over three minutes to less than 20 psi, which is within the range of the differential pressure transducer (Rosemount, Chanhassen, MN) connected across the inlet and outlet.

The temperatures at both ends of the core dropped rapidly in response to the depressurization. T1 (left side, near Pump 1 side in Figure 1) dropped immediately, and T2 (right side) lagged behind by a few minutes. This temperature drop occurred because methane hydrate dissociation is endothermic, and the dissociation was demanding energy from the system. The temperature of the confining fluid immediately outside the sleeve surrounding the sample declined as well with an additional lag in response to the cooling of the sample. The temperature of the cooling bath, although monitored at a location that is remote from the vessel, did not change as a result of the cooling, indicating that the temperature of the fluid in the temperature control jacket was relatively stable over the test. T1 began to rise towards the controlled temperature indicating depletion of hydrate after about 5100 seconds, and the temperature at the right side T2 began to rise towards the control temperature after about 6700 seconds.

The differential pressure, along with the gas production rate, can be used to estimate the effective permeability of the core. Hydrate dissociation releases water and gas, but water is preferentially retained by the water-wet mineral core. Since most of the fluid produced (leaving the core) from the sample was gas (there may have been a small amount of liquid produced), the flow rate and differential pressure provides the needed information to compute the gas relative permeability. High differential pressure is indicative of low effective permeability. The measured differential pressure was noisy over the first 10,000 seconds, corresponding to the time when the temperature at the right side began to rapidly approach the control temperature. This noisy differential pressure likely results from dissociating gas forming in pockets of capillary-held water until sufficient gas is produced to break through the capillary-held water. The smooth differential pressure decline that occurred following the noisy portion indicates that residual methane gas from dissociation and dissolution slowly leaked through the porespace.

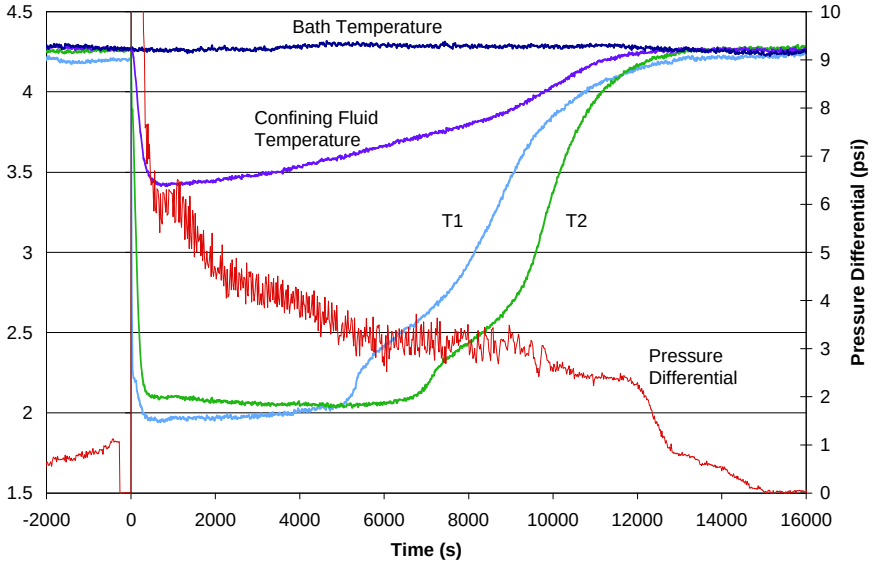

Figure 4. Pressures, temperatures, and differential pressure during the depressurization test.

The volume of fluids (primarily gas and some water) produced was measured at the high-pressure syringe pump. The temperature of the pump was measured using a type T thermocouple to allow computation of the quantity (moles) of gas. The number of moles was computed using density values from NIST [*Lemmon et al.*, 2005] based on measured temperatures and pressures is shown in Figure 5.

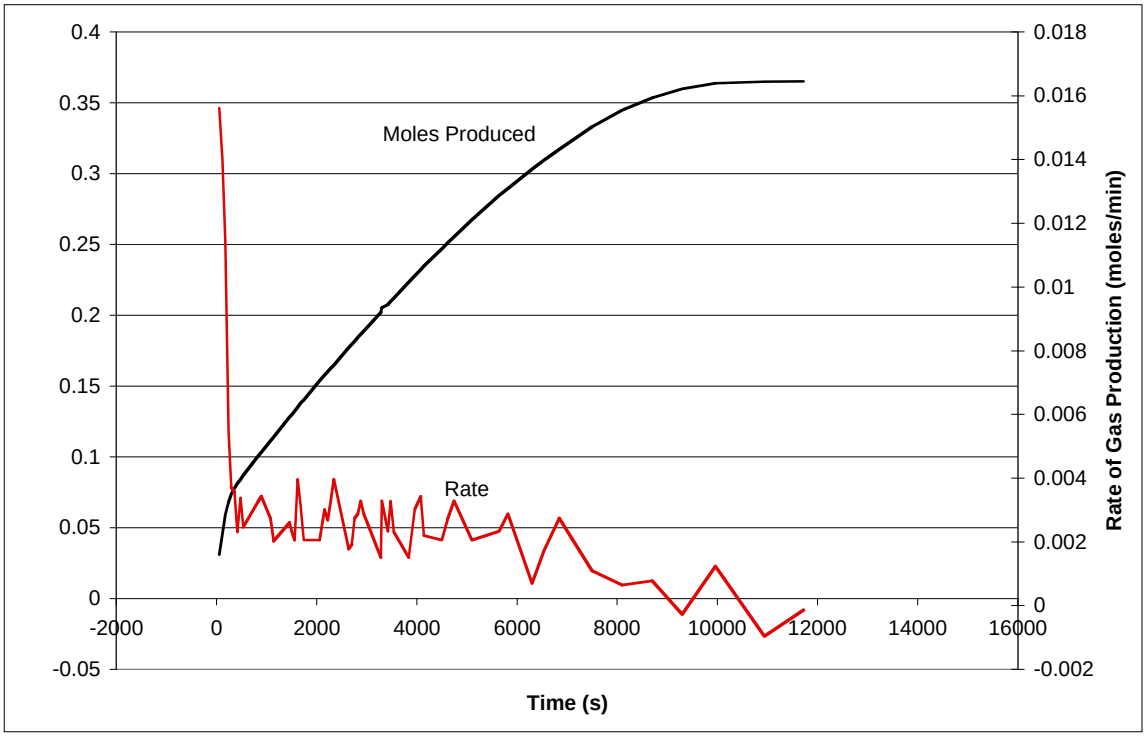

Figure 5. Gas produced and rate of gas production during the test.

X-ray CT scans of 10 locations evenly spaced throughout the core sample were taken approximately every ten minutes during the depressurization test. The CT scans provide a spatially resolved measure of the sample density at approximately 4 million locations in the sample (~78,500 - 195 x 195 x 3000 micron voxels per slice, 51 slices). Changes in the density at a location arise from 1) changes in phase occupancy within the pore space (hydrate, gas, water), 2) gas evolution from hydrate (when the gas leaves the system resulting in a decrease in mass), 3) water leaving the system, and 4) solid mineral rearranging or leaving the system. With few exceptions, the mineral grains were reasonably well cemented and held in place over the duration of the test by the combined cement and confining stress, thus changes in density from this are not considered. The other three processes could have happened during the test. Figure 6 shows the initial sample density and the changes in density at the 3 locations over the first 207 minutes (12,420 s) of the test. Locations 1 and 5 in the figure are from the lower porosity left side, and Locations 10 is from the higher porosity right side.

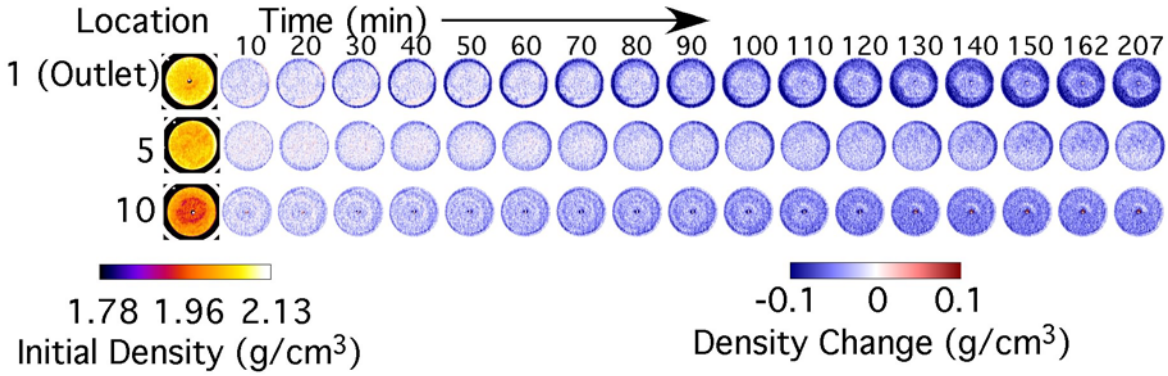

Figure 6. Sample density and density changes over time for three locations. Left-most column shows the initial density distribution of the sample at 3 slices with brighter colors indicating higher density. In the columns to the

right of that, changes in density over time are shown with darker blue indicating larger changes.

History matching results

The ϕ and S_H of the two regions were treated as perturbation parameters (i.e., four in total) that were determined from the history matching process as the ones minimizing the differences between observations and numerical predictions. Given the relatively large number of the perturbation parameters, the values of all other parameters and variables were fixed in the course of the optimization process.

Figure 7 shows the comparison between the measured and predicted mass of collected gas during the dissociation experiment. The match between the two data sets is very good, and the excellent agreement is attributed (at least partly) to both the experimental component of this study and the earlier studies (Anderson et al., 2008; Moridis et al., 2010) that provided good estimates of a large number of the properties and parameters used in the history-matching study, thus minimizing the number of perturbation parameters and enhancing the history-matching process. The optimized perturbation parameters were ϕ = 0.34 and S_H = 0.152 in Region 1 of the core, and ϕ = 0.37 and S_H = 0.270 in Region 2.

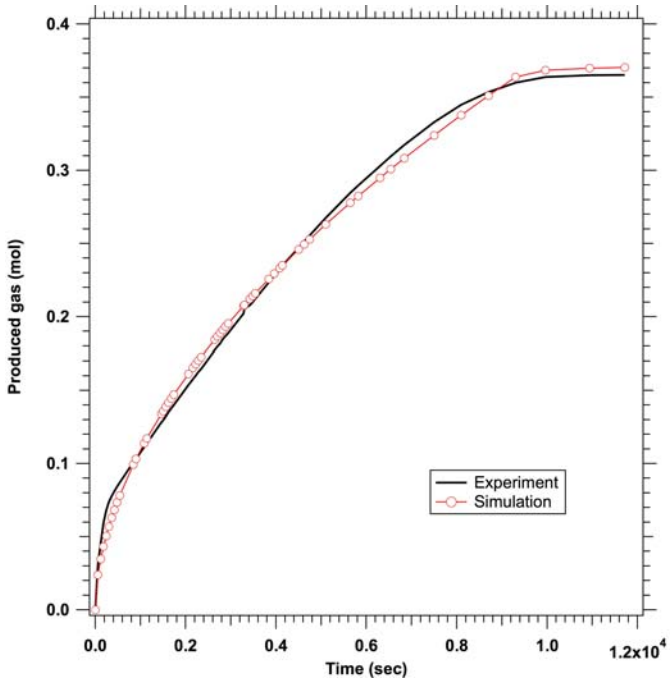

Figure 7. Comparison between measurements and optimized (history-matched) predictions of produced gas from the core dissociation experiment.

Discussion

Our hypotheses were that 1) initial dissociation would occur from heat present in the system until the equilibrium temperature was attained, 2) hydrate would dissociate from the outside in as a result of heat transfer, and 3) hydrate dissociation would be preferential on the outlet (left) side of the sample due to its proximity to the outlet.

Pressure, Differential Pressure, Temperature

Early in the dissociation, the temperature of the sample (T1 and T2) decreased to 2.0 and 2.1^{o}C (Figure 4) at the two core measurement locations. These temperatures are consistent with methane hydrate dissociation at the different pressures at these two locations. As expected, the temperature of the confining fluid declined to a value between the bath temperature and the sample temperature. T1, closer to the fluid outlet (left) end at lower pressure, was cooler, and the dissociation near T1 ended earlier than the dissociation near T2 at the right side of the system. This would be expected from such a system because of the pressure gradient across the core. The fluid outlet side (at lower pressure and larger driving force)

would be expected to dissociate more rapidly than the distant side at higher pressure. The shape of the temperature curves is unusual in that when the dissociation near the thermocouples ended, the temperature rapidly increased for a short time, then the increase was moderated prior to a final rapid increase in temperature. In tests on other systems, temperatures more smoothly approached the control temperature once the dissociation near the thermocouple was complete [*Kneafsey et al.*, 2007; *Kneafsey et al.*, 2009b]. This nonuniform increase may result from the sample geometry and the thermocouple location. The thermocouple was placed to give an indication of the temperature inside the sample. Because the dissociation was caused by depressurization and the effective permeability of the sample was low, the oversized hole drilled for the thermocouple was initially a dissociation surface and later a significant gas flow pathway in the sample. The later moderation of the temperature rise was likely due to the continuing dissociation of hydrate axially inward from the thermocouple. This is supported by the fact that the initial temperature rise at T2 is at about 7,000 seconds, whereas the gas production levels off at about 10,000 seconds.

Gas Produced

The response upon the initiation of depressurization was a rapid collection of fluid (mostly gas) over the first 5 minutes. This was due to gas expansion in the sample and some dissociation as indicated by the immediate temperature decline, and the duration of period is likely due to the low effective permeability of the rock. A high effective permeability would have allowed the gas to rapidly expand and be collected, however this took some time because the effective permeability was so low. During the initial depressurization, gas production is not dependent on heat transfer from outside the sample, but rather on heat contained in the system components (hydrate, water, and mineral grains) and the sample rapidly cooled to the equilibrium temperature at the prevailing pressure. Following the initial depressurization, heat transfer occurs from the outside in. This results in a system that is heat-transfer controlled and yields a decreasing rate of dissociation because heat must be transferred through a growing layer of hydrate-depleted porous media.

X-ray CT

We expected to see 1) initial dissociation (indicated by a slight density decrease) throughout the sample resulting from hydrate dissociation from heat contained in the sample, 2) a hydrate dissociation front that moved radially inward over time resulting from heat transfer from the temperature controlled outer boundary, and 3) faster dissociation at the lower pressure end. In Figure 6 we see a slight density decrease over the entire core sample at 10 minutes, but we also see a larger density decrease at the outer radii of the core from heat transfer from the confining fluid. The temperature of the confining fluid begins to drop very soon (about 40 seconds) after the depressurization begins, indicating heat is being transferred to the sample at that time. We were not able to capture by CT the initial dissociation by itself indicated by the temperature and gas production data shown in Figures 4 and 5, and our first scan at 10 minutes shows a combination of initial dissociation throughout the core and thermally induced dissociation at the outer radii of the core. If we examine Slice 5 over the duration of the test, we clearly see an inwardly moving dissociation front. The less dense outer layer grows in size throughout the test. This behavior is consistent to some extent over the entire core. The behavior at Location 10 (right end) is somewhat different in that initially the dissociation proceeded radially, but then more uniform dissociation occurred across the profile. Heat transfer to the core through the PVC endcaps also occurred during this test although the thermal conductivity of PVC is lower than nitrile and the thickness of the PVC was significantly greater.

Conclusions

A preserved sample of hydrate-bearing sandstone from the Mount Elbert Test Well was dissociated by depressurization while monitoring the internal temperature of the sample in two locations and the density changes at high spatial resolution using x-ray CT scanning. Hydrate dissociation in the Mount Elbert core occurred primarily as hypothesized; initially throughout the sample as a result of depressing the pressure below the stability pressure, and then from the outside in as a result of heat transfer. Numerical modeling of the test yielded a gas production curve that closely follows the experimentally measured curve. In order to make this match however, slight modifications were needed in the initial parameters including porosity and hydrate saturation. These differences are under investigation.

Acknowledgements

This work was supported by the Assistant Secretary for Fossil Energy, Office of Oil and Natural Gas, through the National Energy Technology Laboratory, of the U.S. Department of Energy under Contract No. DE-AC02-05CH11231. Grain size distributions and mineralogy courtesy of Kyle Littlefield and Kelly Rose of the NETL.

References

Anderson, B.J., Wilder, J.W., Kurihara, M., White, M.D., Moridis, G.J., Wilson, S.J., Pooladi-Darvish, M., Masuda, Y., Collett, T.S., Hunter, R.B., Narita, H., Rose, K. and Boswell, R., 2008. Analysis of Modular Dynamic Formation Test Results From the Mount Elbert-01 Stratigraphic Test Well, Milne Point Unit, North Slope, Alaska**,** paper presented at the 6th International Conference on Gas Hydrates, Vancouver, British Columbia, Canada, July 6-10, 2008.

Boswell, R., et al. (2010), Geologic controls on gas hydrate occurrence in the Mount Elbert prospect, Alaska North Slope, *Marine and Petroleum Geology, In Press, Corrected Proof.*

Clarke, M.A., and Bishnoi, P.R., 2000. Determination of the Intrinsic Rate of Methane Gas Hydrate Decomposition", *Chem. Eng. Sci.*, **55**, 4869.

Hunter, R. B., et al. Mount Elbert Gas Hydrate Stratigraphic Test Well, Alaska North Slope: Overview of scientific and technical program, *Marine and Petroleum Geology, In Press, Corrected Proof.*

Kim, H.C., Bishnoi, P.R., Heidemann, R.A., and Rizvi, S.S.H., 1987. Kinetics of Methane Hydrate Decomposition, *Chem. Eng. Sci.*, **42**(7), 1645.

Kneafsey, T. J., et al. (2007), Methane Hydrate Formation and Dissociation in a Core-Scale Partially Saturated Sand Sample, *JPSE*, *56*, 108-126.

Kneafsey, T. J., et al. (2009a), Analysis of core samples from the BPXA-DOE-USGS Mount Elbert gas hydrate stratigraphic test well: Insights into core disturbance and handling, *Marine and Petroleum Geology*, *In Press, Corrected Proof.*

Kneafsey, T. J., et al. (2009b), Laboratory measurements on core-scale sediment and hydrate samples to predict reservoir behavior, in *Natural gas hydrates—Energy resource potential and associated geologic hazards*, edited by T. Collett, et al., pp. 705–713.

Kowalsky, M. B., and Moridis, G.J., 2007, Comparison of kinetic and equilibrium reactions in simulating the behavior of gas hydrates, *Energy Conversion and Management*, **48**, 1850, doi:10.1016/j.enconman.2007.01.017 (LBNL-63357).

Lemmon, E. W., et al. (2005), Thermophysical Properties of Fluid Systems - NIST Chemistry WebBook, NIST Standard Reference Database Number 69, in *http://webbook.nist.gov*, edited, National Institute of Standards and Technology.

Milkov, A. V. (2004), Global estimates of hydrate-bound gas in marine sediments: how much is really out there?, *Earth Science Reviews*, *66*, 183–197.

Moridis, G.J., Kowalsky, M.B., and Pruess, K., 2008. TOUGH+HYDRATE v1.0 User's Manual: A Code for the Simulation of System Behavior in Hydrate-Bearing Geologic Media, Report LBNL-00149E, Lawrence Berkeley National Laboratory, Berkeley, CA.

Moridis, G. J., and E. D. Sloan (2007), Gas production potential of disperse low-saturation hydrate accumulations in oceanic sediments, *Energy Conversion and Management*, *48*(6), 1834-1849.

Moridis, G.J., S. Silpngarmlert, M.T. Reagan, T.S. Collett, and K. Zhang, Gas Production From a Cold, Stratigraphically Bounded Hydrate Deposit at the Mount Elbert Site, North Slope, Alaska, In press, Journal of Marine and Petroleum Geology, 2010 (doi: 10.1016/j.marpetgeo.2010.01.005, LBNL-3005E).

National Resource Council (2004), *Charting the future of methane hydrate research in the United States*, 192 pp.

Sloan, E. D., et al. (1998), Quantifying Hydrate Formation and Kinetic Inhibition, *Ind. Eng. Chem. Res.*, *37*, 3124-3132.

Sloan, E. D., and C. A. Koh (2008), *Clathrate Hydrates of Natural Gases*, 3 ed., 721 pp., CRC Press, Taylor and Francis Group.

van Genuchten, M.Th., 1980. A Closed-Form Equation for Predicting the Hydraulic Conductivity of Unsaturated Soils", *Soil Sci. Soc.*, 44, 892.

White, M., 2008. Personal communication.

Zhang, K., and Moridis, G.J., 2008. A Domain Decomposition Approach for Large-Scale Simulations of Coupled Processes in Hydrate-Bearing Geologic Media**,** paper presented at the 6th International Conference on Gas Hydrates, Vancouver, British Columbia, Canada, July 6-10, 2008.